Structural Insights into BAF47 and BAF155 Complex Formation

Li Yan, Si Xie, Yongming Du and Chengmin Qian

School of Biomedical Sciences, *The University of Hong Kong, Hong Kong SAR, China*

Correspondence to Chengmin Qian: *School of Biomedical Sciences, The University of Hong Kong, 21 Sassoon Road, Pokfulam, Hong Kong. cmqian@hku.hk.*
http://dx.doi.org/10.1016/j.jmb.2017.04.008
Edited by M. Guss

Abstract

Mammalian BAF complexes are a subfamily of SWI/SNF ATP-dependent chromatin remodelers that dynamically modulate chromatin structure to regulate fundamental cellular processes including gene transcription, cell cycle control, and DNA damage response. So far, many distinct BAF complexes have been identified with polymorphic assemblies of up to 15 subunits from 29 genes. The evolutionarily conserved BRG1/BRM, BAF47, and BAF155/BAF170 form a stable complex that carries out essential chromatin remodeling activity and therefore have been regarded as the core components of BAF complex. Here, we first confirmed that SWIRM domain of BAF155 is responsible for its interaction with BAF47 and then narrowed down the SWIRM-binding region in BAF47 to the Repeat 1 (RPT1) domain. We further presented the high-resolution crystal structure of SWIRM/RPT1 complex. Extensive mutagenesis experiments together with isothermal titration calorimetry and NMR titrations were performed to corroborate the interactions observed in crystal structure. Overall, we demonstrated that BAF155 SWIRM is a modular domain involved in BAF47 interaction, which is functionally distinct from other characterized SWIRM domains that possess DNA binding activity.

Introduction

SWI/SNF (referred to as BRG1/BRM-associated factors in mammalian) complex, as the first identified chromatin remodeling complex, can utilize the energy of ATP hydrolysis to alter chromatin structure, thereby spatiotemporally controlling genomic DNA accessibility to nuclear machinery. So far, 15 BAF subunits have been identified in mammals, and variant subunits can assemble into different combinations that contain either BRG1 or BRM as the catalytic ATPase. It has been well documented that distinct combinatorial assembly of BAF complex produces functional diversity [1–3]. BAF complex regulates the transcription of a large number of target genes and thus plays an essential role in many developmental processes including cardiac development and nervous system development, maintaining pluoripotency in embryonic stem cells (ESCs) and promoting somatic cell reprogramming [4,5]. Pluripotency interactome analyses have identified that esBAF complex functionally associates with Oct4 and Nanog, which greatly facilitates somatic cell reprogramming and helps the induced pluripotent stem cells maintain pluripotency [6,7]. Overexpression of BAF155 and BRG1 in mouse embryonic fibroblasts significantly enhances Oct4-, Sox2-, Klf4-, and c-Myc-mediated reprogramming [8]. In addition, BAF complexes have also been implicated in DNA damage response [9]. BAF complex was shown to accumulate at DNA damage sites induced by laser microirradiation and promote γH2AX induction [10,11]. Another study has demonstrated that BRIT1, an early DNA damage response factor, can help recruit BAF complex to DNA double-strand break sites to relax the nearby chromatin structure, which eventually facilitates other DNA repair factors' access to double-strand break sites [12].

Recent cancer genome sequencing studies have revealed that components of human BAF complex are among the most frequently mutated genes in a variety of tumors [13,14]. BAF47 mutations occur almost 100% in rhabdoid tumors, and PBAF subunit BAF180 is mutated in 41% of renal cell carcinomas.

More broadly, mutations in genes encoding BAF subunits have been identified in over 20% of all human cancers [13–15]. However, the molecular mechanism underlying the contributions of high frequency of BAF subunit mutations to human cancers remains largely unknown.

Although the subunit composition of mammalian BAF complex is very diverse, most BAF complexes contain a subset of core subunits including BRG1/BRM, BAF155/170, and BAF47. *In vitro* biochemical analysis has shown that adding BAF47, BAF155, and BAF170 to BRG1 stimulates its ATPase activity to a level comparable to the intact BAF complex [16]; also, mice lacking BAF47 or BAF155 or BRG1 die at early embryonic stage [17–20], underscoring the essential roles of these core subunits in diverse BAF complexes and in early embryogenesis. Although BAF complex has been extensively studied over the past decades, the molecular mechanism by which these BAF essential subunits interact to form the core regulatory machinery is currently lacking.

BAF47 is a well-known *bona fide* tumor suppressor that is mutated in almost all aggressive rhabdoid tumors predominantly occurring to infants and young children [21,22]. Several recent studies have shown that BAF47 (SNF5 in yeast) plays a critical role in maintaining BAF complex integrity [23–25]. Loss of BAF47 resulted in substantially decreased levels of the BAF complex as observed in a number of rhabdoid cell lines. On the other hand, re-expression of BAF47 in BAF47-deficient cells dramatically increased the incorporation of BAF subunits including Brg1, BAF155/BAF170, and BAF250a into BAF complexes. Interestingly, a previous study has revealed that SS18-SSX evicts SS18 and BAF47 to form an altered BAF complex in human synovial sarcoma, but the process can be reversible, and wild-type BAF complex can be reassembled after increasing the protein level of wild-type SS18 [26]. In addition, BAF47 has been reported to directly bind to HIV-1 integrase to regulate the viral integration [27]. Compared to BAF47, BAF155 and its paralog BAF170 are less frequently mutated in cancers. BAF155 shares a high degree of sequence similarity with BAF170 but has a non-redundant role at the different stages of development. In mouse embryonic stem cells, the ESC-specific BAF complex is characterized by the presence of BRG1, BAF155, and BAF60a and the absence of BRM, BAF170, and BAF60c [7,28]. In contrast, both BAF155 and BAF170 are present in human embryonic stem cells, and knockdown of BAF170 led to the loss of pluoripotency [29]. Besides, BAF155 and/or BAF170, acting as scaffold proteins, have been demonstrated to maintain the integrity of BAF complex by protecting other BAF subunits including BAF47 and BRG1 from proteasomal degradation [30,31]. In this study, we first confirmed that BAF155 and BAF47 form a protein complex. We further identified that BAF155 SWIRM domain interacts directly with BAF47 Repeat 1 (RPT1) domain. The crystal structure of BAF155 SWIRM domain bound to BAF47 RPT1 reveals extensive interactions in which electrostatic interactions dominate, whereas hydrophobic interactions make an additive contribution. Mutagenesis together with isothermal titration calorimetry (ITC) and NMR binding studies validated the importance of these interactions.

Results

BAF155 SWIRM domain binds directly to BAF47 RPT1 domain

Phelan *et al.* have previously demonstated that BAF155 and BAF47 can be co-purified from human cells, suggesting that these two proteins physically interact with each other [16]. In another study, Sohn *et al*. have reported that SWIRM domain of BAF155 is required for the interaction with BAF47 by using yeast two-hybrid assay [30]. To further clarify this observation, we performed co-immunoprecipitation assay upon overexpression of Myc-tagged BAF47 with Flag-tagged full-length BAF155 or Flag-tagged BAF155 SWIRM-truncated mutant or Flag-tagged BAF155 SWIRM domain in HEK293T cells. As shown in Fig. 1a, Flag-tagged BAF155 full-length protein but not the SWIRM-truncated mutant could interact with myc-tagged BAF47. On the other hand, Flag-tagged BAF155 SWIRM domain readily co-purified with BAF47, supporting that SWIRM domain of BAF155 is responsible for the interaction with BAF47. Next, we carried out *in vitro* pull-down assay to map the region of BAF47 that is responsible for BAF155 SWIRM domain interaction. We first prepared various BAF47 fragments encompassing all three well-defined domains: the N-terminal winged helix domain and two repeat domains (RPT1 and RPT2). *In vitro* glutathione *S*-transferase (GST) pull-down assays using GST-tagged BAF155 SWIRM domain indicated that the SWIRM domain specifically interacts with BAF47 RPT1 domain but not with other fragments (Fig. 1b). Analytical gel-filtration analysis also supported that BAF155 SWIRM domain forms a stable complex with BAF47 RPT1 domain (Fig. S1). Interestingly, the peak position of BAF155 SWIRM and BAF47 RPT1 complex on analytical gel filtration corresponds to the calculated molecular weight of ~40 KDa. Protein SDS-PAGE gel of the eluted peak fraction indicated that SWIRM forms a complex with RPT1 with 1:1 stoichiometry in solution, revealing that the complex contains a heterotetramer with two SWIRM and two RPT1 domains. Analytical gel-filtration analyses also confirmed that BAF47 RPT1 alone exists as a dimer, whereas BAF155 SWIRM alone is a monomer in solution (Fig. S1).

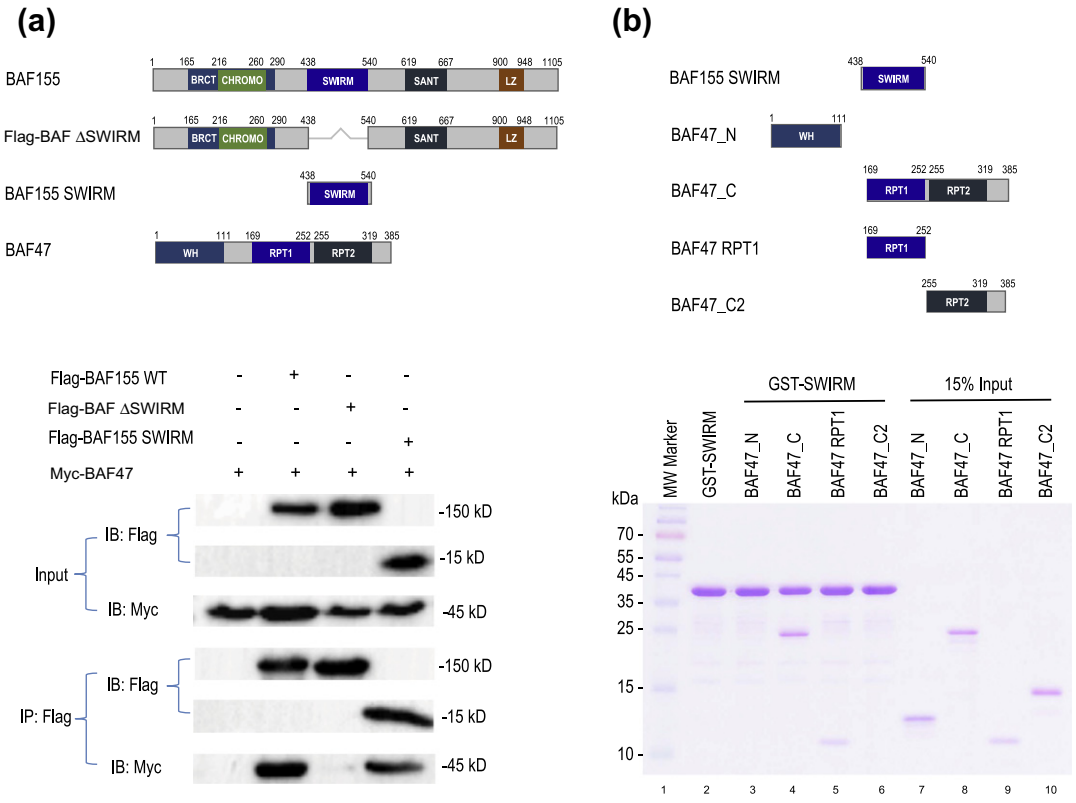

Fig. 1. BAF155 SWIRM domain interacts with BAF47 RPT1 domain. (a) Schematic diagram of BAF155 and BAF47 fragments used in co-immunoprecipitation experiments are indicated in the upper panel. Results from co-IP assay supported that BAF155 SWIRM domain is required for the interaction with BAF47. Co-IP experiments were carried out with different Flag-tagged BAF155 proteins and Myc-tagged BAF47 in HEK293T cells. Cell lysates were subjected to Flag immunoprecipitation using anti-Flag beads. After extensive washing, precipitated proteins were eluted with buffer containing 50 mM Tris–HCl (pH 7.5), 150 mM NaCl, 1 mM EDTA, 1% NP40, and 1 mg/mL Flag peptide. Flag-tagged BAF155 and Myc-tagged BAF47 were probed by indicated anti-Flag and anti-Myc antibodies, respectively. (b) Schematic diagram of BAF155 and BAF47 fragments and results from domain-mapping experiments indicate that BAF155 SWIRM domain binds to the BAF47 RPT1 domain. The GST pull-down assay was performed using recombinant GST-tagged BAF155 SWIRM domain as the bait. GST-tagged SIWRM was immobilized, washed, and then incubated, respectively, with untagged BAF47_N, BAF47_C, BAF47_RPT1, and BAF47_C2. Proteins were subsequently eluted from the beads (lanes 2–6) and visualized in SDS-PAGE gel. Lanes 7–10 correspond to 15% input of different BAF47 fragments and loaded as control.

Crystal structure of BAF155 SWIRM domain bound to BAF47 RPT1 domain

We went on to determine the crystal structure of BAF155 SWIRM domain in complex with BAF47 RPT1 domain at 2.05-Å resolution (Fig. 2a, crystallographic statistics are given in Table 1). Consistent with analytical gel-filtration results, the overall structure is a heterotetramer in which two BAF47 RPT1 domains dimerize in a head-to-tail manner; at the same time, each RPT1 subunit forms a heterodimer with a BAF155 SWIRM domain. BAF155 SWIRM domain comprises five α helices highly similar to other SWIRM domain structures (Fig. S2) [32–34]. BAF47 RPT1 domain consists of a two-stranded antiparallel β sheet followed by two α helices (Fig. S2). The compact architecture of RPT1 domain is stabilized by a hydrophobic core built by two α helices packing against each other on the same side of the β sheet. Residues Phe218, Leu222, and Leu226 from helix α1 and residues Phe233, Ile237, Ile241, and Ile245 from helix α2 interact extensively with the hydrophobic patch formed by residues Ile189, Leu191, Met193, and Ile195 of β1 strand and residues Leu200, Phe204, and Trp206 of β2 strand (Fig. S3a). It is worth noting that a structural similarity search from the DALI server (DALI Z scores around 3.5) revealed that the overall fold of BAF47 RPT1 domain most closely resembles WNK1 auto-inhibitory domain (PDB ID: 2LRU) and human PLAA PLUC domain (PDB ID: 2K89). WNK1 auto-inhibitory domain contains a three-antiparallel β strands followed by two α helices, while human PLAA PLUC domain has a compact architecture consisting of four β strands followed by two α helices. Interestingly, these three

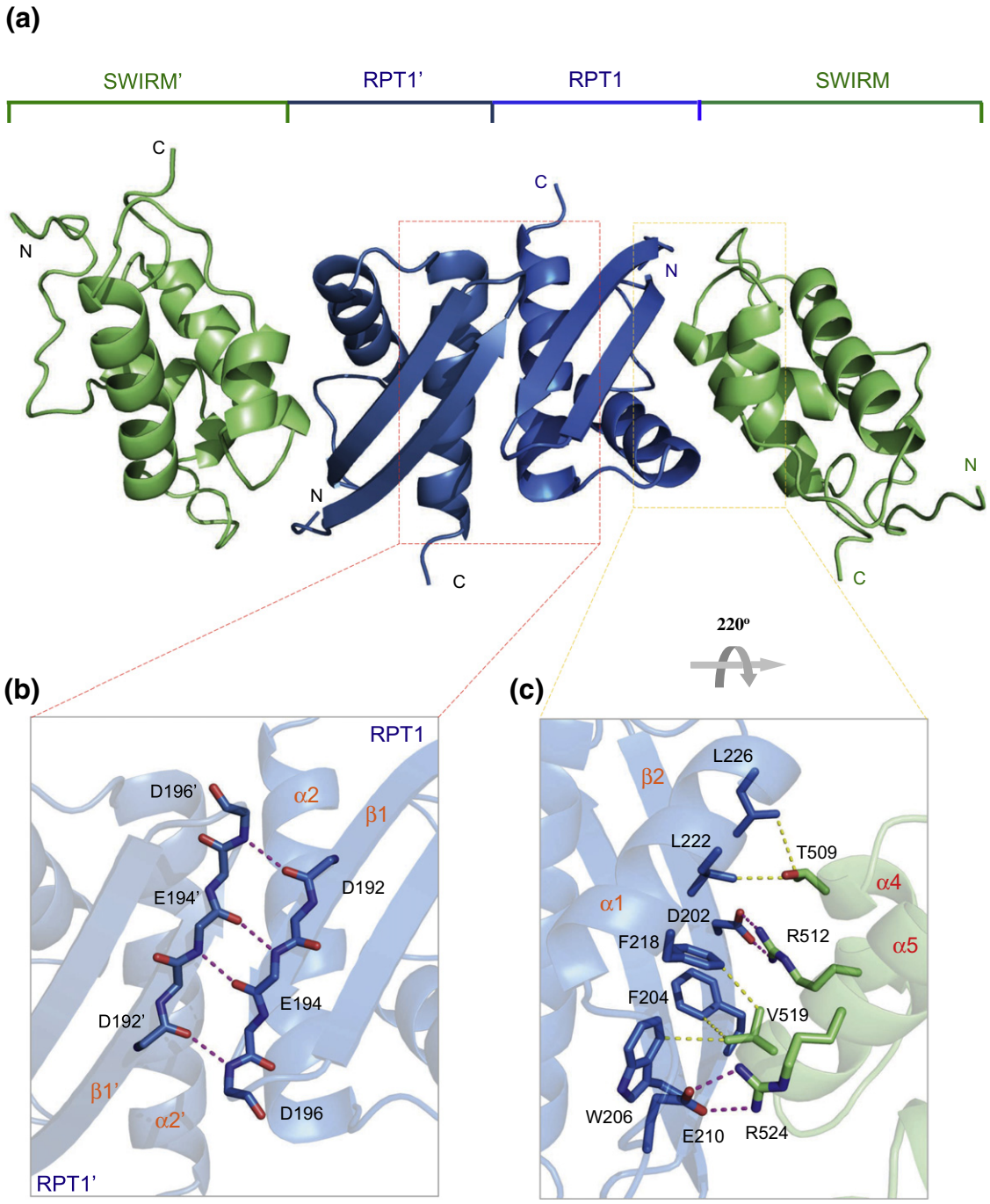

Fig. 2. Three-dimensional crystal structure of the BAF155 SWIRM domain bound to BAF47 RPT1 domain. (a) BAF155 SWIRM and BAF47 RPT1 domain form a symmetric dimer of heterodimer in which RPT1 dimerizes in a head-to-tail manner; also, each RPT1 subunit (colored in marine and sky blue, where the labels with superscript prime refer to the other subunit) binds to a SWIRM domain (colored in lime). (b) Dimerization of RPT1 is stabilized by intersubunit hydrogen bonds of antiparallel β sheet formed between two RPT1 β1 strands. Residues involved in main-chain to main-chain hydrogen bonds formation are shown in stick model and labeled. (c) Detailed interaction between BAF155 SWIRM and BAF47 RPT1 domain. Residues that form the binding interface are depicted as stick models and labeled. Hydrogen bonds and salt bridges are shown in magenta dashed lines; hydrophobic interactions are in yellow dashes.

domains share the similar structural fold but have very distinct biological functions (Fig. S3b–d) [35,36].

In the complex structure, the head-to-tail dimerization of RPT1 is mediated mainly by hydrogen bonds between main-chain atoms of β1 strand of

Table 1. Crystallographic data collection and refinement statistics.

	SWIRM–RPT1 complex
PDB ID	5GJK
Data collection	
Wavelength	0.9793 Å
Space group	*P*62 2 2
Unit cell *a*, *b*, *c* (Å)	*a* = *b* = 80.518 Å, *c* = 200.952 Å
Resolution (Å; highest resolution shell)	50.00–2.05 (2.09–2.05)
Observed reflections	461,259
Unique reflections	25,126
Completeness (%)	100.0 (100.0)
R_{merge}	0.105 (0.478)
I/	34.9 (8.0)
Redundancy	18.4 (18.6)
B-factor (Å ^{2})	28.8
Refinement	
Resolution (Å)	39.47–2.05 (2.13–2.05)
No. of reflections	24,965 (2405)
R_{work}/R_{free} (%)	19.5/21.3
No. of non-H atoms	1458
Protein	1322
Water	136
B-factors (Å^2)	31.2
RMSD	
Bond lengths (Å)	0.007
Bond angles (°)	0.85
Ramachandran favored (%)	98.1
Ramachandran allowed (%)	1.9

each RPT1 subunit. As shown in Fig. 2b, β1 strands of both RPT1 subunits form an intersubunit antiparallel β sheet, characteristic of four main-chain to main-chain hydrogen bonds among residues D192, E194, and D196 of one subunit and residues D196′, E194′, and D192′ of the other subunit (with the prime indicating the other subunit). At the same time, helices α2 of two RPT1 subunits pack against each other and orient in the opposite directions; the favorable interactions between these two α-helix dipoles stabilize the dimerization of RPT1 as well.

As mentioned above, the overall structure consists of two SWIRM/RPT1 heterodimers that associate via dimerization of RPT1. Close examination of the SWIRM/RPT1 heterodimer structure revealed that both electrostatic and hydrophobic interactions contribute to the formation of the stable heterodimer of RPT1 and SWIRM, burying the total solvent-accessible surface area of 1398.2 Å^2 (Fig. S4). The C-terminal α4-turn-α5 motif of SWIRM domain interacts extensively with β2-loop-α1 of RPT1 domain (Fig. 2c). Notably, SWIRM domain residue Arg512 of helix α4 and Arg524 of helix α5 form two ion pairs with RPT1 residue Asp202 of β2 and Glu210 in the loop between β2 and α1, respectively. The side chain of SWIRM residue Val519 is in hydrophobic contact with RPT1 aromatic residues including Phe204, Trp206, and Phe218; also, side-chain methyl group of residue Thr509 from SWIRM helix α4 makes hydrophobic contact with methyl groups of Leu222 and Leu226 from RPT1 helix α1.

Measurement of the binding of BAF155 SWIRM domain to BAF47 RPT1 domain

To corroborate the interactions observed in the crystal structure, we generated a number of BAF155 SWIRM mutants and quantitatively evaluated the effect of mutations on binding to RPT1 by ITC. BAF155 SWIRM binds to RPT1 with a K_d of 0.12 ± 0.01 μM (Fig. 3a–c and Fig. S5). Single mutation of SWIRM Arg512 or Arg524 with Ala reduced binding affinities 60- to 70-fold, and double mutation of SWIRM Arg512 and Arg524 to Ala led to the abrogation of interactions with RPT1. Mutation of SWIRM Val519 to Gly that affects the hydrophobic interaction caused about 20-fold reduction in binding affinity. These observations are in complete agreement with the structural findings. We also applied NMR titration to further verify the effect of mutagenesis on the binding. As shown in superimposed 2D ^{15}N-heteronuclear single quantum coherence (HSQC) spectra of BAF47 RPT1 (Fig. 3d), upon the addition of the BAF155 SWIRM domain, a number of RPT1 amide resonances showed progressive line-broadening effect and eventually disappeared, while a set of new peaks emerged when the molar ratio reached 1:1, indicating a slow exchange between RPT1 free form and RPT1/SWIRM complex form. This conclusion was further confirmed by reciprocal NMR titration of RPT1 into ^{15}N-labeled SWIRM solution, as many cross peaks disappeared, owning to the serious line broadening (Fig. 3e). Similar patterns but with much smaller resonance perturbations have also been observed when titrating SWIRM V519G mutant, R512A mutant, or R524A mutant into a solution of ^{15}N-RPT1 (Fig. S6). Under the same 1:1 molar ratio, fewer new peaks were shown in RPT1 ^{15}N-HSQC spectra after adding these SWIRM mutants when comparing the titration result of wild-type SWIRM. No obvious line broadening or chemical shift perturbation was observed when adding SWIRM R512A/R524A double mutant to ^{15}N-RPT1 solution, suggesting that double mutation of R512A and R524A disrupted the RPT1–SWIRM interaction, while these single mutations caused a reduction in binding affinity. NMR titration results agree well with ITC measurement and structural observations.

Our previous structure-based study has highlighted that human ADA2α SWIRM domain binds to chromosomal DNA [32]; also, yeast Swi3 SWIRM domain was reported to have a similar DNA binding activity [33]. Therefore, we tested if BAF155 SWIRM domain has the DNA binding activity. ITC shows that BAF155 has no detectable interaction with 12-bp double-stranded DNA fragment (Fig. 4a). NMR titration reveals no obvious chemical shift changes or line-broadening effect when titrating

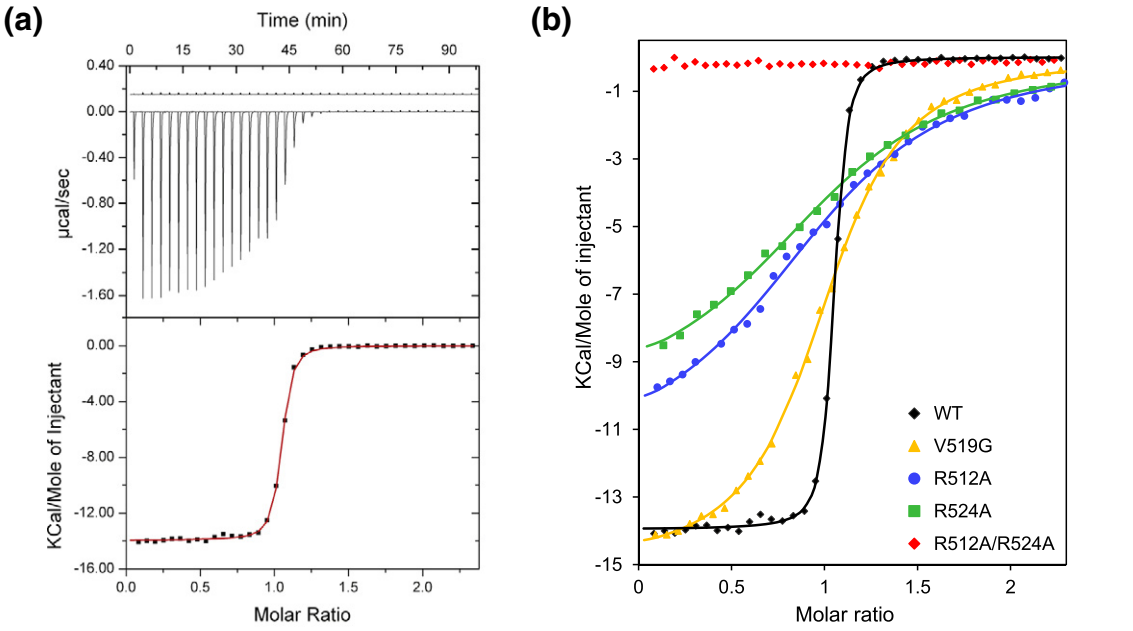

(c)

Protein	Titrant	K_d (µM)	n	ΔH (kcal/mol)	TΔS (kcal/mol)
RPT1	SWIRM WT	0.12 ± 0.01	1.02	-13.94 ± 0.43	-4.50
	SWIRM V519G	2.2 ± 0.1	1.02	-14.98 ± 0.07	-7.27
	SWIRM R512A	6.9 ± 0.4	1.01	-11.88 ± 0.19	-4.83
	SWIRM R524A	7.9 ± 0.4	1.01	-10.28 ± 0.15	-3.31
	SWIRM R512A/R524A	ND	ND	ND	ND

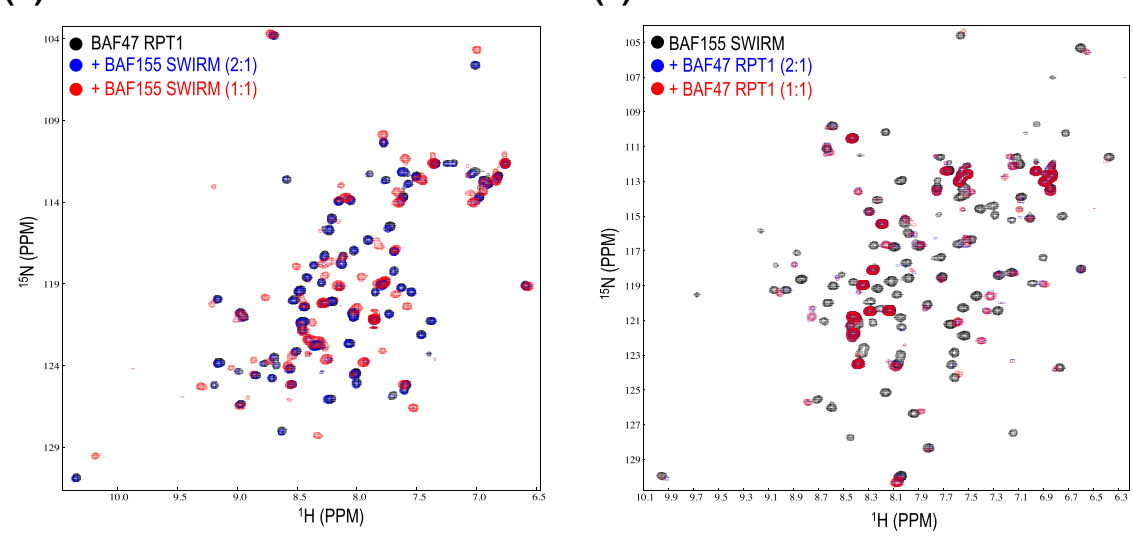

Fig. 3 *(legend on next page)*

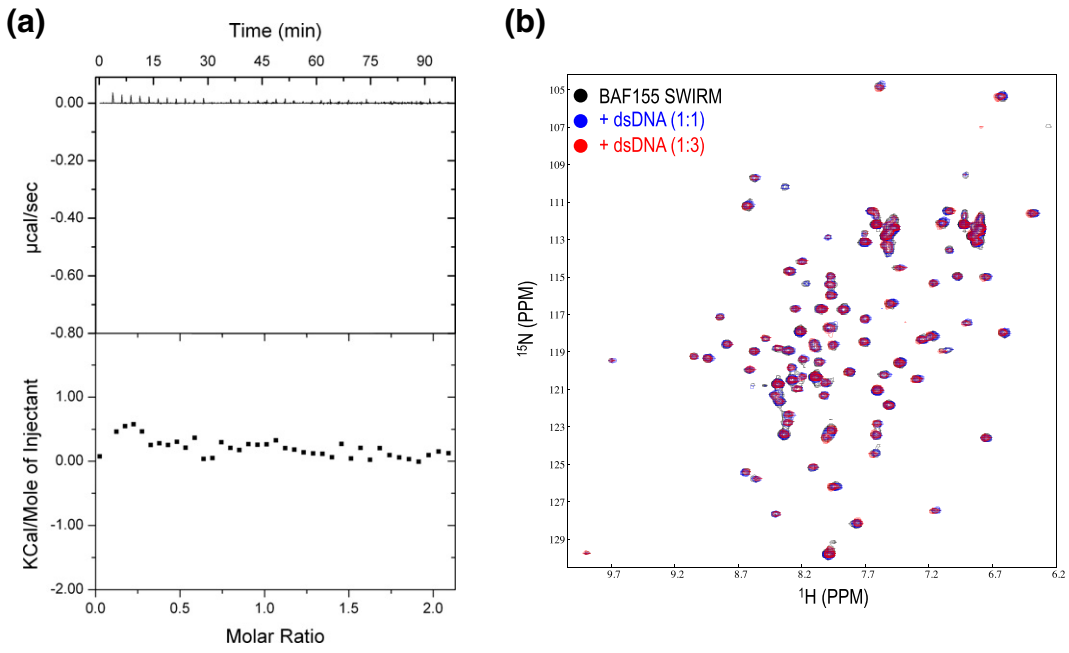

Fig. 4. Binding analysis of SWIRM to a double-stranded DNA fragment. (a) The results of ITC titration reveal that wild-type BAF155 SWIRM domain has no detectable binding to 12-bp dsDNA. (b) Superimposition of 2D ^{15}N-HSQC spectra of SWIRM in the free form (black) *versus* in the presence of dsDNA with molar ratios 1:1(blue) and 1:3 (red).

dsDNA into a solution of ^{15}N-SWIRM with the final molar ratio of dsDNA and SWIRM up to 3:1 (Fig. 4b), indicating that BAF155 SWIRM domain does not bind to dsDNA. A previous report has suggested that BAF complex could bind to architectural DNA [37]; we therefore designed six different types of DNA fragments (the sequence and conformational information is listed in Supplemental Table 1) and performed ITC measurement. Interestingly, none of these DNA fragments showed detectable binding to BAF155 SWIRM (Fig. S7). Taken together, these results suggested that BAF155 SWIRM domain does not possess DNA binding activity.

Discussion

Mammalian BAF complex belongs to SWI/SNF chromatin remodeling family that was originally identified in yeast [38]. Although SWI/SNF complex has lost and gained a number of subunits during evolution, BAF47 and BAF155/BAF170 are evolutionarily conserved and homologous proteins can be found in yeast, flies, plants, and mammals [39]. In addition, BAF47 and BAF155 or BAF170 are present in almost all identified tissue- or cell-type-specific BAF complexes. It has previously been demonstrated that BAF47, BAF155, and BAF170 can form a stable complex [16,30]. Interestingly, this protein complex can further bind to BRG1 and greatly stimulate BRG1 chromatin remodeling activity, suggesting that these core components are required for efficient chromatin remodeling activity. BAF47 and BAF155 contain a number of modular domains including RPT, Chromo, SWIRM, and SANT that have been implicated in mediating protein–protein or protein–DNA interactions. For example, BAF47 RPT1 domain was first identified to bind to HIV integrase and is required for efficient HIV-1 particle production [27,40]. BAF47 RPT1 domain was also shown to interact with c-Myc and may facilitate the transcription of c-Myc target genes. In this study, we provided the structural evidence that BAF47 RPT1 is involved in the stable interaction with BAF155

Fig. 3. Binding analysis of SWIRM wild type and mutants to RPT1. (a) Experimental ITC curves show titration results of wild-type BAF155 SWIRM domain with BAF47 RPT1. (b) ITC fitting curves for the binding of BAF155 SWIRM domain wild type, V519G, R512A, R524A, and R512A/R524A with BAF47 RPT1. The calculated binding affinities and thermodynamic parameters are summarized in (c). (d) Superimposition of 2D ^{15}N-HSQC spectra of ^{15}N-labeled BAF47 RPT1 amide resonances in the free form (black) and in the presence of BAF155 SWIRM with molar ratios 2:1(blue) and 1:1(red). (e) Overlay of 2D ^{15}N-HSQC spectra of SWIRM in the free form (black) and in the presence of RPT1 with molar ratios 2:1 (blue) and 1:1(red).

SWIRM domain. We observed that BAF170 SWIRM domain binds equally well to BAF47 RPT1 (data not shown), which is not surprising considering that it shares over 95% sequence identity with BAF155 SWIRM, and all residues important for RPT1 binding are highly conserved.

SWIRM domain is a conserved protein module found in a number of chromosomal proteins including chromatin remodeling complex SWI/SNF (BAF and PBAF in mammals), histone lysine demethylase LSD1, and transcriptional adaptor ADA2 of histone acetyltransferase SAGA. Previous structure-based studies have highlighted human ADA2α, and yeast Swi3 SWIRM domains have DNA binding activity [32,33], while several studies have also suggested that some subtypes of SWIRM domains may be involved in other functions distinct from DNA binding [30,34]. Indeed, in this study, we show that BAF155 SWIRM domain is involved in the physical interaction with BAF47 RPT1. Notably, residues in BAF155 SWIRM and BAF47 RPT1 critical for their recognition are highly conserved in their yeast counterparts Swi3 and Snf5 (Fig. S8), suggesting that this might be an evolutionarily conserved property of SWIRM domain. Intriguingly, the C-terminal helix-turn-helix motif of yeast Swi3 SWIRM domain was mapped to bind to nucleic acids [33], while we show that BAF155 SWIRM does not bind to DNA, and its C-terminal helix-turn-helix motif directly participates in RPT1 binding. It would be interesting to test if Swi3 SWIRM domain binds directly to Snf5.

In conclusion, we reported the crystal structure of BAF47 RPT1 bound to BAF155 SWIRM domain and provided the molecular basis of the complex formation of two BAF complex core subunits BAF47 and BAF155.

Materials and Methods

Plasmid construction, protein expression, and purification

The human BAF155 SWIRM domain (residue 438–540) was cloned into pGEX-6p1 plasmid as an N-terminal GST-tagged protein, and BAF47_N (residue 3–111), BAF47_C (residue 169–385), BAF47 RPT1 (residue 169–252), and BAF47_C2 (residue 255–385) were cloned into pET28a or home-engineered pRSF-SUMO vectors. Fusion proteins were expressed in *Escherichia coli* strain Rosetta DE3 (Novagen) and purified via either GSTrap HP column or nickel-NTA affinity column, followed by size-exclusion and/or ion exchange chromatography. Various BAF155 SWIRM mutants were generated using QuikChange site-directed mutagenesis kit (Stratagene) and confirmed by DNA sequencing. Uniformly ^{15}N-labeled proteins were prepared by growing bacteria in minimal medium with $^{15}NH_4Cl$ as the sole nitrogen source. Protein NMR samples were prepared in a 20-mM phosphate buffer of pH 6.8 containing 100 mM NaCl, 2 mM DTT, and 10% D_2O (vol/vol).

For co-immunoprecipitation experiments, human full-length BAF155 (residue 1–1105), BAF155 ΔSWIRM (Δ438–540), and BAF155 SWIRM (residue 438–540) were amplified by PCR and ligated into pcDNA3 vector with N-terminal Flag tag. Human BAF47 (residue 1–385) was ligated into pcDNA3.1 vector with N-terminal Myc tag.

Co-immunoprecipitation assay

Flag-tagged full-length BAF155 or Flag-tagged BAF155 ΔSWIRM or Flag-tagged SWIRM was co-transfected with Myc-tagged BAF47 in HEK293T cells using Lipofectamine 2000 (Invitrogen). HEK293T cells were harvested 48 h after transfection. The cells were lysed in NP40 buffer [50 mM Tris (pH 7.5), 150 mM NaCl, 1 mM EDTA, and 1% NP40] supplemented with PMSF and protease inhibitor cocktail (Roche). Clarified cell lysates were subjected to Flag immunoprecipitation using anti-Flag beads (Sigma), and 10% cell lysate was saved as input control. The beads were washed three times with NP40 buffer after incubation with cell lysate. Immunoprecipitated proteins were eluted with NP40 buffer supplemented with 1 mg/mL Flag peptide. For immunoblotting, the eluted proteins were transferred from SDS-PAGE gels to PVDF membrane. Flag-tagged BAF155 proteins and Myc-tagged BAF47 protein were probed by indicated anti-Flag and anti-Myc antibodies, respectively.

In vitro pull-down assay

In vitro GST pull-down assays were performed to map the interaction of BAF155 SWIRM domain with various BAF47 fragments. GST-tagged BAF155 SWIRM domain was immobilized on glutathione agarose beads first, washed with the PBS buffer containing 2 mM DTT, and then incubated, respectively, with untagged BAF47_N, BAF47_C, BAF47_RPT1, and BAF47_C2 at 4 °C for 30 min. Mixtures were washed five times with the washing buffer and then eluted with 20 mM Tris–HCl (pH 8.0), 150 mM NaCl, and 5 mM reduced glutathione. The proteins were detected in SDS-PAGE gel with Coomassie-blue staining. Untagged BAF47 fragments do not bind to either GST-tag or glutathione resin.

Crystallization and structure determination

Crystals of the BAF155 SWIRM domain in complex with BAF47 RPT1 were obtained at 298 K with

the vapor diffusion hanging drop method by mixing 1 μl of the protein complex solution with 1 μl of crystallization solution [0.9 M sodium phosphate monobasic monohydrate and potassium phosphate dibasic (pH 5.4)]. All diffraction data were collected at 100 K at SSRF beamline BL17U. The native crystal diffracted to 2.05 Å. All data were processed with HKL-2000 [41]. The crystals belong to space group *P*6222 with unit cell dimensions of $a = b = 80.518$ Å, $c = 200.952$ Å, $\alpha = \beta = 90°$, $\gamma = 120°$. The complex structure was solved by molecular replacement using Phaser-MR in Phenix and with a previously determined SWIRM structural model (PDB: 2FQ3) as the searching template. The molecular replacement solution was used subsequently for the structure refinement using Phenix Refine with manual model building in COOT [42,43]. Final X-ray data collection and refinement statistics are summarized in Table 1.

NMR titration

All NMR spectra were acquired at 298 K on a Bruker Avance 600 MHz NMR spectrometer with cryoprobe. The titration was performed by recording a series of 2D ^{15}N-HSQC spectra on uniformly ^{15}N-labeled RPT1 domain (about 0.2 mM) in the presence of different amounts of SWIRM ranging from 0 to 0.5 mM. Similar procedures were carried out for recording 2D ^{15}N-HSQC spectra on uniformly ^{15}N-labeled SWIRM in the presence of RPT1. NMR data were processed by NMRPipe and subsequently analyzed by NMRView [44,45].

ITC

Calorimetric experiments were conducted at 25 °C with a MicroCal ITC200 instrument. Protein samples were prepared in the buffer containing 20 mM sodium phosphate (pH 6.8) and 100 mM sodium chloride. Titrations were performed as follows: 50–100 μM BAF155 SWIRM wild-type or mutant solution was transferred into the sample cell, and 1 preliminary injection of 0.5 μl of 0.5–1 mM BAF47 RPT1 domain was followed by about 38 injections of 1 μl. The delay time between the injections was 150 s. Data were analyzed using MicroCal Origin software. Similar procedures were carried out for titrating different types of DNA fragments with BAF155 SWIRM.

Accession number

The atomic coordinates of BAF155 SWIRM in complex with BAF47 RPT1 have been deposited at the protein data bank with accession code **5GJK**.

Acknowledgments

We wish to acknowledge the use of the Shanghai synchrotron radiation (beamline BL17U) for X-ray data collection and Bruker Avance 600 MHz NMR spectrometer with cryoprobe installed in the Chemistry Department of HKU for NMR data collection. We thank Dr. HZ Sun for facilitating NMR data collection. This study is supported by grants from Hong Kong Research Grants Council (17127715 and 775712) to C. Qian.

Author contributions: C. Qian conceived the project. L. Yan conducted most of the experiments. S. Xie and Y. Du contributed to the data collection and the discussion. C. Qian wrote the manuscript with the input from all authors.

Appendix A. Supplementary Data

Supplementary data to this article can be found online at http://dx.doi.org/10.1016/j.jmb.2017.04.008.

Received 19 December 2016;
Received in revised form 16 April 2017;
Accepted 18 April 2017
Available online 21 April 2017

Keywords:
BAF47;
BAF155;
SWIRM;
RPT1;
X-ray crystallography

Abbreviations used:
ESC, embryonic stem cell; RPT1, Repeat 1; ITC, isothermal titration calorimetry; GST, glutathione *S*-transferase; PDB, Protein Data Bank; NMR, nuclear magnetic resonance; HSQC, heteronuclear single quantum coherence; dsDNA, double-stranded DNA.

References

[1] C.R. Clapier, B.R. Cairns, The biology of chromatin remodeling complexes, Annu. Rev. Biochem. 78 (2009) 273–304.
[2] C. Kadoch, G.R. Crabtree, Mammalian SWI/SNF chromatin remodeling complexes and cancer: mechanistic insights gained from human genomics, Sci. Adv. 1 (2015) e1500447.
[3] J.A. Lessard, G.R. Crabtree, Chromatin regulatory mechanisms in pluripotency, Annu. Rev. Cell Dev. Biol. 26 (2010) 503–532.

[4] L. Ho, G.R. Crabtree, Chromatin remodelling during development, Nature 463 (2010) 474–484.
[5] A. Gaspar-Maia, A. Alajem, E. Meshorer, M. Ramalho-Santos, Open chromatin in pluripotency and reprogramming, Nat. Rev. Mol. Cell Biol. 12 (2011) 36–47.
[6] J. Wang, S. Rao, J. Chu, X. Shen, D.N. Levasseur, T.W. Theunissen, et al., A protein interaction network for pluripotency of embryonic stem cells, Nature 444 (2006) 364–368.
[7] L. Ho, J.L. Ronan, J. Wu, B.T. Staahl, L. Chen, A. Kuo, et al., An embryonic stem cell chromatin remodeling complex, esBAF, is essential for embryonic stem cell self-renewal and pluripotency, Proc. Natl. Acad. Sci. USA 106 (2009) 5181–5186.
[8] N. Singhal, J. Graumann, G. Wu, M.J. Arauzo-Bravo, D.W. Han, B. Greber, et al., Chromatin-remodeling components of the BAF complex facilitate reprogramming, Cell 141 (2010) 943–955.
[9] P.M. Brownlee, C. Meisenberg, J.A. Downs, The SWI/SNF chromatin remodelling complex: its role in maintaining genome stability and preventing tumourigenesis, DNA Repair (Amst) 32 (2015) 127–133.
[10] L. Izhar, B. Adamson, A. Ciccia, J. Lewis, L. Pontano-Vaites, Y. Leng, et al., A systematic analysis of factors localized to damaged chromatin reveals PARP-dependent recruitment of transcription factors, Cell Rep. 11 (2015) 1486–1500.
[11] J.H. Park, E.J. Park, H.S. Lee, S.J. Kim, S.K. Hur, A.N. Imbalzano, et al., Mammalian SWI/SNF complexes facilitate DNA double-strand break repair by promoting gamma-H2AX induction, EMBO J. 25 (2006) 3986–3997.
[12] G. Peng, E.K. Yim, H. Dai, A.P. Jackson, I. Burgt, M.R. Pan, et al., BRIT1/MCPH1 links chromatin remodelling to DNA damage response, Nat. Cell Biol. 11 (2009) 865–872.
[13] C. Kadoch, D.C. Hargreaves, C. Hodges, L. Elias, L. Ho, J. Ranish, et al., Proteomic and bioinformatic analysis of mammalian SWI/SNF complexes identifies extensive roles in human malignancy, Nat. Genet. 45 (2013) 592–601.
[14] L.A. Garraway, E.S. Lander, Lessons from the cancer genome, Cell 153 (2013) 17–37.
[15] A.H. Shain, J.R. Pollack, The spectrum of SWI/SNF mutations, ubiquitous in human cancers, PLoS One 8 (2013) e55119.
[16] M.L. Phelan, S. Sif, G.J. Narlikar, R.E. Kingston, Reconstitution of a core chromatin remodeling complex from SWI/SNF subunits, Mol. Cell 3 (1999) 247–253.
[17] S. Bultman, T. Gebuhr, D. Yee, C. La Mantia, J. Nicholson, A. Gilliam, et al., A Brg1 null mutation in the mouse reveals functional differences among mammalian SWI/SNF complexes, Mol. Cell 6 (2000) 1287–1295.
[18] A. Klochendler-Yeivin, L. Fiette, J. Barra, C. Muchardt, C. Babinet, M. Yaniv, The murine SNF5/INI1 chromatin remodeling factor is essential for embryonic development and tumor suppression, EMBO Rep. 1 (2000) 500–506.
[19] J.K. Kim, S.O. Huh, H. Choi, K.S. Lee, D. Shin, C. Lee, et al., Srg3, a mouse homolog of yeast SWI3, is essential for early embryogenesis and involved in brain development, Mol. Cell. Biol. 21 (2001) 7787–7795.
[20] C.W. Roberts, M.M. Leroux, M.D. Fleming, S.H. Orkin, Highly penetrant, rapid tumorigenesis through conditional inversion of the tumor suppressor gene Snf5, Cancer Cell 2 (2002) 415–425.
[21] I. Versteege, N. Sevenet, J. Lange, M.F. Rousseau-Merck, P. Ambros, R. Handgretinger, et al., Truncating mutations of hSNF5/INI1 in aggressive paediatric cancer, Nature 394 (1998) 203–206.
[22] J.A. Biegel, J.Y. Zhou, L.B. Rorke, C. Stenstrom, L.M. Wainwright, B. Fogelgren, Germ-line and acquired mutations of INI1 in atypical teratoid and rhabdoid tumors, Cancer Res. 59 (1999) 74–79.
[23] X. Wang, R.S. Lee, B.H. Alver, J.R. Haswell, S. Wang, J. Mieczkowski, et al., SMARCB1-mediated SWI/SNF complex function is essential for enhancer regulation, Nat. Genet. 49 (2017) 289–295.
[24] P. Sen, J. Luo, A. Hada, S.G. Hailu, M.L. Dechassa, J. Persinger, et al., Loss of Snf5 induces formation of an aberrant SWI/SNF complex, Cell Rep. 18 (2017) 2135–2147.
[25] A. Dutta, M. Sardiu, M. Gogol, J. Gilmore, D. Zhang, L. Florens, et al., Composition and function of mutant Swi/Snf complexes, Cell Rep. 18 (2017) 2124–2134.
[26] C. Kadoch, G.R. Crabtree, Reversible disruption of mSWI/SNF (BAF) complexes by the SS18-SSX oncogenic fusion in synovial sarcoma, Cell 153 (2013) 71–85.
[27] G.V. Kalpana, S. Marmon, W. Wang, G.R. Crabtree, S.P. Goff, Binding and stimulation of HIV-1 integrase by a human homolog of yeast transcription factor SNF5, Science 266 (1994) 2002–2006.
[28] L. Ho, R. Jothi, J.L. Ronan, K. Cui, K. Zhao, G.R. Crabtree, An embryonic stem cell chromatin remodeling complex, esBAF, is an essential component of the core pluripotency transcriptional network, Proc. Natl. Acad. Sci. USA 106 (2009) 5187–5191.
[29] X. Zhang, B. Li, W. Li, L. Ma, D. Zheng, L. Li, et al., Transcriptional repression by the BRG1-SWI/SNF complex affects the pluripotency of human embryonic stem cells, Stem Cell Rep. 3 (2014) 460–474.
[30] D.H. Sohn, K.Y. Lee, C. Lee, J. Oh, H. Chung, S.H. Jeon, et al., SRG3 interacts directly with the major components of the SWI/SNF chromatin remodeling complex and protects them from proteasomal degradation, J. Biol. Chem. 282 (2007) 10,614–10,624.
[31] J. Chen, T.K. Archer, Regulating SWI/SNF subunit levels via protein–protein interactions and proteasomal degradation: BAF155 and BAF170 limit expression of BAF57, Mol. Cell. Biol. 25 (2005) 9016–9027.
[32] C. Qian, Q. Zhang, S. Li, L. Zeng, M.J. Walsh, M.M. Zhou, Structure and chromosomal DNA binding of the SWIRM domain, Nat. Struct. Mol. Biol. 12 (2005) 1078–1085.
[33] G. Da, J. Lenkart, K. Zhao, R. Shiekhattar, B.R. Cairns, R. Marmorstein, Structure and function of the SWIRM domain, a conserved protein module found in chromatin regulatory complexes, Proc. Natl. Acad. Sci. USA 103 (2006) 2057–2062.
[34] M. Yoneyama, N. Tochio, T. Umehara, S. Koshiba, M. Inoue, T. Yabuki, et al., Structural and functional differences of SWIRM domain subtypes, J. Mol. Biol. 369 (2007) 222–238.
[35] T.M. Moon, F. Correa, L.N. Kinch, A.T. Piala, K.H. Gardner, E.J. Goldsmith, Solution structure of the WNK1 autoinhibitory domain, a WNK-specific PF2 domain, J. Mol. Biol. 425 (2013) 1245–1252.
[36] Q.S. Fu, C.J. Zhou, H.C. Gao, Y.J. Jiang, Z.R. Zhou, J. Hong, et al., Structural basis for ubiquitin recognition by a novel domain from human phospholipase A2-activating protein, J. Biol. Chem. 284 (2009) 19,043–19,052.
[37] W. Wang, T. Chi, Y. Xue, S. Zhou, A. Kuo, G.R. Crabtree, Architectural DNA binding by a high-mobility-

group/kinesin-like subunit in mammalian SWI/SNF-related complexes, Proc. Natl. Acad. Sci. USA 95 (1998) 492–498.
[38] F. Winston, M. Carlson, Yeast SNF/SWI transcriptional activators and the SPT/SIN chromatin connection, Trends Genet. 8 (1992) 387–391.
[39] J.I. Wu, J. Lessard, G.R. Crabtree, Understanding the words of chromatin regulation, Cell 136 (2009) 200–206.
[40] A. Morozov, E. Yung, G.V. Kalpana, Structure-function analysis of integrase interactor 1/hSNF5L1 reveals differential properties of two repeat motifs present in the highly conserved region, Proc. Natl. Acad. Sci. USA 95 (1998) 1120–1125.
[41] T. Otwinowski, W. Minor, Processing of X-ray diffraction data collected in oscillation mode, Methods Enzymol. 276 (1997) 307–326.
[42] P. Emsley, K. Cowtan, Coot: model-building tools for molecular graphics, Acta Crystallogr. 60 (2004) 2126–2132.
[43] P.D. Adams, P.V. Afonine, G. Bunkoczi, V.B. Chen, I.W. Davis, N. Echols, et al., PHENIX: a comprehensive Python-based system for macromolecular structure solution, Acta Crystallogr. D Biol. Crystallogr. 66 (2010) 213–221.
[44] F. Delaglio, S. Grzesiek, G.W. Vuister, G. Zhu, J. Pfeifer, A. Bax, NMRPipe: a multidimensional spectral processing system based on UNIX pipes, J. Biomol. NMR 6 (1995) 277–293.
[45] B.A. Johnson, Using NMRView to visualize and analyze the NMR spectra of macromolecules, Methods Mol. Biol. 278 (2004) 313–352.